



Surface urban heat islands in 932 urban region agglomerations in China during the morning and before midnight: spatial-temporal changes, drivers, and simulation

Yuanzheng Li^{a,b}, Zhizhi Feng^a, Lin Li^c, Tiancheng Li^a, Fuyin Guo^a, Jing Wei^d, Yi Yan^e and Lan Wang^f

^aSchool of Resources and Environment, Henan University of Economics and Law, Zhengzhou, China; ^bAcademician Laboratory for Urban and Rural Spatial Data Mining of Henan Province, Henan University of Economics and Law, Zhengzhou, China; ^cSchool of Resources and Environment, Qingdao Agricultural University, Qingdao, China; ^dDepartment of Atmospheric and Oceanic Science, Earth System Science Interdisciplinary Center, University of Maryland, College Park, MD, USA; ^eKey Laboratory of Resources Conversion and Pollution Control of the State Ethnic Affairs Commission, College of Resources and Environmental Science, South-Central Minzu University, Wuhan, China; ^fKey Research Institute of Yellow River Civilization and Sustainable Development & Collaborative Innovation Center on Yellow River Civilization jointly built by Henan Province and Ministry of Education, Henan University, Kaifeng, China

ABSTRACT

Research was insufficient on the surface urban heat islands (SUHIs) in China during the morning and before midnight. Therefore, we studied the spatio-temporal variations and ten determinants of SUHI intensities (SUHIs) at ~10:30 am and ~10:30 pm of 932 urban region agglomerations in the five ecological regions in China and further simulate these SUHIs using the machine learning algorithm. The main findings were as follows. (1) The daytime SUHIs in all regions were largest in the summer, and when the humid regions had higher SUHIs than other regions. The maximum SUHIs were usually significantly positively correlated with the minimum ones. (2) The SUHIs were significantly partially correlated with the enhanced vegetation index, nighttime light intensity, PM_{2.5}, albedo, population density, precipitation, urban area size and landscape shape index in many or a few cases. (3) The root-mean-square errors of simulated daytime and nighttime SUHIs were mostly less than 1.22 and 2.00 °C, respectively.

ARTICLE HISTORY

Received 2 February 2022
Accepted 22 May 2022


KEYWORDS

Urban thermal environment; land surface temperature; remote sensing; general regression neural network; influencing factors

1. Introduction

China has experienced rapid urbanization in recent decades. Its urbanization rate had increased from 10.64% in 1949 to 63.89% in 2020. The increase trend will continue until 2050 (United Nations, Department of Economic and Social Affairs (UN DESA) 2014).

CONTACT Lan Wang  wlsunshinelz@163.com

 Supplemental data for this article can be accessed online at <https://doi.org/10.1080/10106049.2022.2082552>

© 2022 Informa UK Limited, trading as Taylor & Francis Group

Nowadays, more than 901.99 million populations live in cities in China. Urbanization could cause higher temperatures in urban regions than outskirts and villages, called the urban heat island (UHI). The UHI has direct or indirect impacts on the urban thermal environment, human temperature-related comfort, health and mortality, urban precipitation, energy use, air quality, etc. The research methods for UHIs mainly include the observation method by meteorological stations (Shen et al. 2020), in-situ fixed-points (Sfîcă et al. 2018) or moving transects (Silva et al. 2018), numerical simulation method (Chen et al. 2022) and remote sensing method (Zhou et al. 2019). Remote sensing can provide consistent and repeatable observations of land surface temperatures (LSTs) at various spatial and temporal scales. Close relationships existed between the LSTs and near-surface air temperatures (Marzban et al. 2018). Therefore, the surface urban heat island (SUHI) derived by remote sensing has been widely accepted and analyzed (Zhou et al. 2019). The SUHIs were complex and serious in China. The maximum and minimum SUHI intensities (SUHIs) can be 8.93 and -9.91°C in China, respectively (Li et al. 2019a).

Some research has studied the spatial-temporal changes and their drivers of SUHI at the global scale and the national scale in China (Table S1). Their study objects were usually 419 (Peng et al. 2012), 9500 (Chakraborty and Lee 2019), 193,090 (Clinton and Gong 2013) global cities or urban clusters, thirty large provincial capital cities and above (Zhou et al. 2014; Cao et al. 2016) or about three hundred Prefecture-level cities and above (Yang et al. 2019; Niu et al. 2021a; Yao et al. 2021). The SUHIs and footprints (FPs) were two widely adopted indicators to quantify SUHI. The SUHIs were generally defined as the differences of LSTs between the cities or urban centers and their surrounding rural or outskirt regions (Cao et al. 2016; Lai et al. 2018; Peng et al. 2018). These regions were usually derived by the land use, the proportion of impervious surface and waterbodies, altitude, distance from the cities, etc. (Zhou et al. 2014; Peng et al. 2018; Yao et al. 2021). The FPs of SUHIs were defined as the cities and their nearby regions whose LSTs were larger than the mean LSTs in the corresponding rural regions (Zhou et al. 2015) or the ellipse areas that crossed the fitted Gaussian surfaces (Yang et al. 2019). The cities in the world or China were usually grouped due to the different climatic zones (Lai et al. 2018; Chakraborty and Lee 2019), biome areas (Zhang et al. 2010), ecological regions (Li et al. 2019a; Li et al. 2019b), or land cover majority in the rural regions (Clinton and Gong 2013). This was because the SUHIs of cities in different groups have different spatial-temporal change laws and influencing factors. Many influencing factors of SUHIs have been analysed, including the differences between cities or city centres and outskirts or villages for the altitude (ΔAlt) (Zhou et al. 2014), aerosol optical depth (ΔAOD) (Cao et al. 2016; Li et al. 2019b; Lai et al. 2021), $\text{PM}_{2.5}$ ($\Delta\text{PM}_{2.5}$) (Niu et al. 2021b), enhanced vegetation index (ΔEVI) (Zhou et al. 2016; Yao et al. 2021), vegetation fractional cover (ΔVFC) (Peng et al. 2018), several landscape metrics (Yang et al. 2017), nighttime light intensity (ΔNLI) (Zhou et al. 2014; Yao et al. 2017), normalized difference vegetation index (ΔNDVI) (Cao et al. 2016; Lai et al. 2018), population density (ΔPD) (Li et al. 2019b), proportion of impervious surface (ΔPIS) (Zhou et al. 2014; Yao et al. 2021), and while-sky albedo (ΔWSA) (Cao et al. 2016; Yao et al. 2018), cropland fraction of the rural background (CF) (Cao et al. 2016), latitude (Zhang et al. 2010; Clinton and Gong 2013), longitude, height/width ratio (HWR), the height of the tallest object, the lower surfaces (Clinton and Gong 2013), anthropogenic heat flux (AHF) (Ma et al. 2021), humidity index (HI) (Li et al. 2019b; Ma et al. 2021), mean air temperature (MAT) (Zhou et al. 2016; Yao et al. 2018), morphological continuity (MC) (Ma et al. 2021), morphological continuity fractal dimension (MFD) (Ma et al. 2021), mean solar radiation (MSR) (Ma et al. 2021), mean wind speed (MWS) (Yao et al. 2018; Yao et al. 2021), urban area size (UAS) (Zhou et al. 2014; Li et al. 2019b), specific humidity (SH) (Ma et al. 2021), total

population (T_Pop) (Zhou et al. 2014; Li et al. 2019b), total precipitation (T_Pre) (Cao et al. 2016; Yao et al. 2021), total sunshine duration (T_SD) (Cao et al. 2016; Yao et al. 2021), area-weighted mean shape index (AWMSI), dispersion index (DI), entropy and Moran's I (Liu et al. 2021) etc. Most research used the Pearson's (Zhou et al. 2014; Yao et al. 2021) or Spearman's rank correlation analysis (Zhou et al. 2016; Yang et al. 2019) and linear regression (Zhou et al. 2014; Chakraborty and Lee 2019) to explore the relationships between the SUHIs or FPs and their influencing factors. The previous research has made important progress that could provide significant references for subsequent studies. Nevertheless, some issues still existed. First, the spatial-temporal changing rules of SUHIs were scarcely studied in the cities with various (mega, large, medium and small) sizes with different ecological contexts of China during the morning and before midnight, including the mean, maximum and minimum SUHIs together with their occurring seasons, and ranges of SUHIs, etc. (Table S1). Meanwhile, the outdoor activities are frequent during the morning and before midnight. Moreover, many humans live in county towns or county-like towns in China. Second, the influences for SUHIs were insufficiently analysed for these various cities, especially the PM_{2.5}, urban shape, etc. Third, the SUHIs were seldomly simulated using these influencing factors during the morning and before midnight, although this was quite important for the regulation and optimization of the urban thermal environment. Fourth, most research did not make the quality control (QC) of LSTs, which may introduce a certain bias or even errors for SUHI research. How to realize it more effectively and accurately was worth to be explored.

Thus, our objective is to explore the spatial-temporal changes and ten associate determinants of SUHIs during the morning and before midnight (~10:30 pm) in 932 urban region agglomerations in the five regions with different ecological contexts in China and further simulate these SUHIs.

2. Study area and data

2.1. Study area

China was divided into five ecological zones (Figure 1), having considering the different spatial-temporal variation rules and drivers of SUHIs under different contexts (Li et al. 2019a, 2019b). The ecological zones data were provided by the Database of Ecosystem Assessment and Ecological Security Pattern in China, which were identified by considering several factors comprehensively, including the landform, climate, vegetation, human activity, etc. East China belongs to the monsoon climate zone, where it's wet and rainy in the summer while dry and rainy in the winter. Region I, II, IV and V mainly enjoyed the middle and cold temperate zones, warm temperate zone, subtropical zone, and tropical zone, respectively. West China (Region III) is not affected by monsoons and has less precipitation (<400 mm in the whole year). It includes the typical temperate continental climate zone and alpine climate zone (Tibetan Plateau Region).

2.2. Data

Table 1 summarized the main data used in this study. The Terra/MODIS LST data (MOD11A2.006) were derived by the split-window technique. The satellite passes through twice a day, at ~10:30 am and ~10:30 pm. The differences of MODIS LST data were more minor than 1 K in 39 of 47 cases (Wan 2008) and less than 5% in the urban regions compared to the in-situ measured LSTs (Rigo et al. 2006). The MODIS monthly vegetation

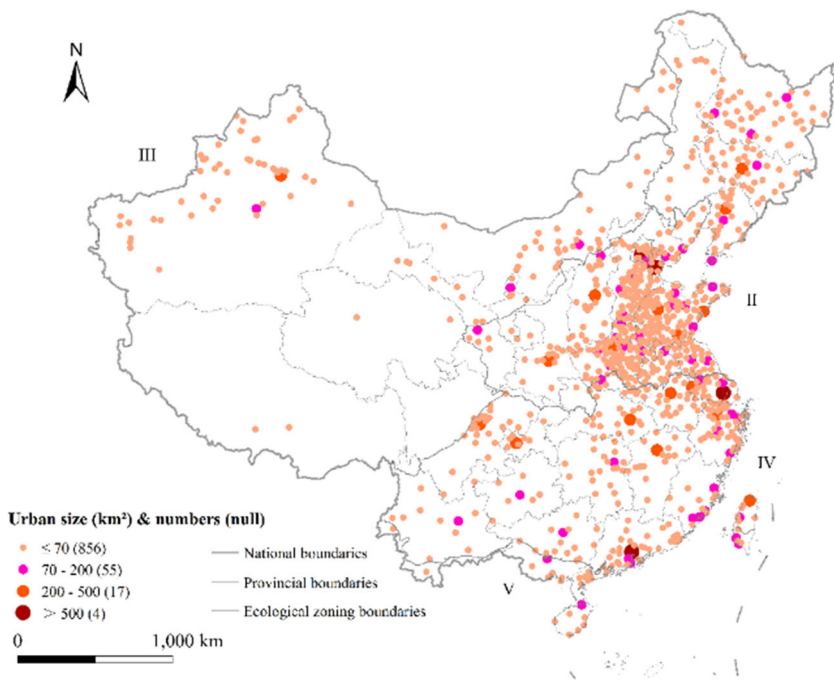


Figure 1. Locations of 932 urban region agglomerations in the five ecological subareas in China.

Table 1. The main data used in this study.

Data	Spatial resolution	Temporal resolution	Source	Time period
Terra/MODIS LST	1 km	8 days	https://search.earthdata.nasa.gov	2014.12–2019.11
Terra/MODIS EVI	1 km	1 month	https://search.earthdata.nasa.gov	2015.12–2016.11
Combined/MODIS Albedo	0.5 km	1 day	https://search.earthdata.nasa.gov	2015.12–2016.11
Land use	1 km	Multi-years	https://www.resdc.cn	2015 & 2020
Elevation	1 km	No	https://www.resdc.cn	No
VIIRS Nighttime light	15 arc seconds	1 year	https://eogdata.mines.edu/products/vnl/	2016
PM _{2.5}	1 km	1 day	https://weijing-rs.github.io/product.html	2015.12–2016.11
Air temperature	1 km	1 month	National Climate Center, China Meteorological Administration	2015.12–2016.11
Precipitation	1 km	1 month	National Climate Center, China Meteorological Administration	2015.12–2016.11
Population	1 km	1 year	https://www.worldpop.org/	2016
Ecological function zones	≤1 km	No	State Key Laboratory of Urban and Regional Ecology, Research Center for Eco-Environmental Sciences, Chinese Academy of Sciences	No

LST and EVI represents the land surface temperature and enhanced vegetation index, respectively; MODIS and VIIRS refer to Moderate Resolution Imaging Spectroradiometer and visible infrared imager radiometer sensor, respectively.

indices (MOD13A3.006) products were integrated by all the 16 days products (MOD13A2) that overlapped the months and employed a weighted temporal average. Only the white-sky albedo for the shortwave band was used due to its high correlation with the black-sky albedo in the MCD43A3.006 product (Peng et al. 2012). The land use data in 2015 and 2020 with

1 km resolution were primarily derived by interpreting the Landsat TM/ETM+ images (Liu et al. 2014). The overall accuracy of classification is more than 91.2% for each land use type (Liu et al. 2014). All the annual visible infrared imager radiometer sensors (VIIRSs) NLIs were set as 0 when their values were negative or larger than the maximum NLI in all urban regions of China or the land use was the waterbodies.

The $PM_{2.5}$ data were collected from the ChinaHighAirPollutants (CHAP) dataset, which were estimated from the MODIS/Terra + Aqua MAIAC AOD products and other auxiliary data using the artificial intelligence method (Wei et al. 2020, 2021). The daily $PM_{2.5}$ estimates agree well with ground-based $PM_{2.5}$ measurements with average root-mean-square errors (RMSEs) ranging from 10.0 to $18.4 \mu\text{g}/\text{m}^3$. The air temperature and precipitation data were interpolated by the Anuspl 4.3 software using the climate records in more than 2400 weather stations. The Worldpop program could provide high resolution, open and contemporary data in human population distributions (Lloyd et al. 2017), which has been widely accepted and adopted (Mohanty and Simonovic 2021). The ecological function zones were identified mainly based on landforms, water and heat combinations, and vegetation characteristics.

3. Methods

3.1. Quality control of the land surface temperatures

One workflow was proposed to identify these invalid LST pixels (Figure S1). The valid LSTs should be between -90 and 90°C , respectively. Both values should be equal or less to 01 in the 1 & 0 and 3 & 2 bites of the QC data. Moreover, the LST in the pixel should be less than 12 K than its adjacent pixels in most cases by using the search method within eight directions, smaller than 12 and 20 K than the medium and maximum value of its 30 and 50 nearest pixels in the same row using the search method in the horizontal direction, respectively. It should note that all conditions mentioned above were restricted step by step. That meant the output data in the former step were the input data in the next step.

3.2. Definition of urban and rural regions

A two-step aggregation method was developed to extract the urban regions accurately. These classified urban land polygons were first aggregated at a distance of 1.5 km. This threshold could not be larger. Otherwise, some isolated urban regions in humans' traditional understanding turned to be aggregated together. Then these urban lands were dissolved together within the same urban region aggregations. Only the dissolved urban lands with areas large than 6 km^2 were primarily chosen as the study objects, covering the vast majority of cities in the regions with the densest populations or most developed economies in China (Li et al. 2019a). Then, perform these operations again for the above-extracted urban area aggregations. However, the aggregation distance was set as 3.75 km, which was approximately equalling to the distance that people could go in 15 min by bicycle and large enough to merge the scattered urban lands polygons into their belonging urban region agglomerations. The operations mentioned above were done for both the land cover data in 2015 and 2020. Their intersection regions were determined as the final urban region agglomerations.

The rural areas were defined as the buffer zones of these urban region agglomerations with the buffer distance of 5–10 km (Clinton and Gong 2013; Li et al. 2019a), excluding

the construction lands (except rural residential areas), waterbodies, marshlands, pixels with slopes large than 7.5° (Li et al. 2019a), or elevations that are 50 m greater than the maximum elevations or less than the minimum elevations of their corresponding urban region agglomerations, respectively (Imhoff et al. 2010; Zhou et al. 2016; Li et al. 2019a).

3.3. Spatial-temporal variation rules of surface urban heat islands

The SUHIs were defined as the differences of LSTs between the urban and rural regions. It should note that the winter was defined as the period from the December in the previous year to February in this year in our study (Li et al. 2019a). First, we analysed the spatial-temporal rules of mean, maximum, and minimum values, their occurring seasons, and annual ranges of daytime and nighttime SUHIs using the space mapping method and mathematical statistics. Second, the mean comparisons were performed using the nonparametric tests for SUHIs between the daytime and nighttime, among the four seasons and five ecological regions. Third, the Spearman rank correlation coefficients were calculated between the annual maximum and minimum SUHIs during the daytime, nighttime and all-day in each season and the entire year in China and its five ecological regions to quantify whether the maximum and minimum values would occur in the same locations; between the annual daytime and nighttime SUHIs ranges, and between the mean daytime and nighttime SUHIs to explore the relationships between daytime and nighttime SUHIs in each region and period.

3.4. Associated determinants of surface urban heat islands

These considered influencing factors included the differences between urban and rural regions for the mean enhanced vegetation index (ΔEVI), nighttime light intensity (ΔNTI), $\text{PM}_{2.5}$ ($\Delta\text{PM}_{2.5}$), population density (ΔPD), and medium albedo (ΔAlb), urban area size (UAS), total population (T_Pop) in the urban region agglomerations, mean air temperature (MAT) and total precipitation (T_Pre) in the centroids of these urban region agglomerations. The partial correlation coefficients and their significance levels were computed between the SUHIs and their determinants in China and its four regions in the entire year and four seasons. It should note that the urban region agglomerations in regions IV and V were considered together due to a limited number of urban region agglomerations in region V. Moreover, the $\text{PM}_{2.5}$ data could only cover some areas in West China. Therefore, this study could just consider the influencing factors of SUHIs in 47/103 urban region agglomerations in region III.

3.5. Simulation of surface urban heat islands

The SUHIs of China and its four regions in the whole year and four seasons were simulated by the general regression neural network (GRNN) method, which has been universally applied in previous research (Rooki 2016; Li et al. 2021). The GRNN algorithm has strong nonlinear mapping ability, high robustness and fault tolerance and could obtain good simulation results when the samples number is small, and some instability exists. The ratio was set as 4:1 for the training and testing sample sets. Only these determinants that were significantly partially correlated with SUHIs were used as the input data in most cases. All the variables were used in region III during the daytime in the spring and autumn and in the autumn night. This was because no significant partial correlation existed in these three cases. Finally, the RMSEs were calculated to indicate the simulated

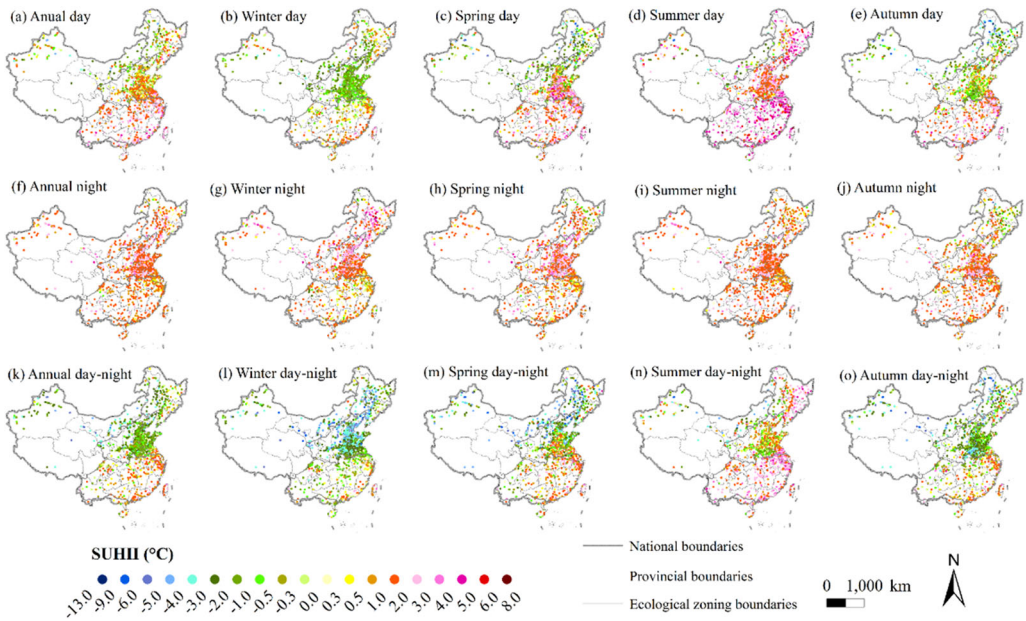


Figure 2. Distribution of the annual and seasonal mean surface urban heat island intensities (SUHIs) during the daytime and nighttime, and the differences between them in China and its five ecological regions during 2015–2019.

accuracies. The procedure was executed 50 times to avoid uncertainties in the process of machine learning and obtain stable simulation results.

4. Results

4.1. Spatio-temporal changes of surface urban heat islands

4.1.1. Spatio-temporal changes of surface urban heat islands during the daytime

The annual mean SUHIs were from 0 to 2 °C and negative in 56.55 and 25.11% urban region agglomerations, respectively (Figures 2a and S2a). These negative values were mainly distributed in North China. The order of regions in SUHIs was $V = IV > II > I > III$, whose values were most from 1 to 3, 1 to 3, 0 to 1, -1 to 1, -2 to 1 °C, respectively (Figures S2a and S3a). The SUHIs showed obvious seasonal variations in China (Figures 2, S2a, and S3a). The values were largest in the summer in all regions when the hot and cold humid regions had higher SUHIs than other regions, mostly from 2.0 to 6.0 °C. The values were less in region II, 77.53% of which were mostly from 1.0 to 3.0 °C; and least in region III, 43.69% were even negative. The SUHIs were least in the winter in regions II, IV and V, and in the Spring and Autumn Seasons in regions I and III. The proportions of the negative season mean SUHIs were 67.92, 44.53 and 33.05% in the winter, spring, and autumn, respectively, mostly distributed in North China.

The largest maximum SUHIs occurred in the hot-humid region V and IV, in which 63.82% SUHIs were from 3 to 5 °C (Figures 3a, S4a, and S5a). The order of the rest regions was region $I > II > III$, in which the maximum SUHIs were most ranging from 3 to 4, 2 to 3 and -4 to 0 °C, respectively. The maximum SUHIs were negative in 32.04% of cities in the dry region III. Moreover, the largest maximum SUHIs were most occurring in the summer in all regions of China, never in the winter in regions II, V and IV, least in the Spring and Autumn Seasons in regions III and I (Figures 3d and S6a).

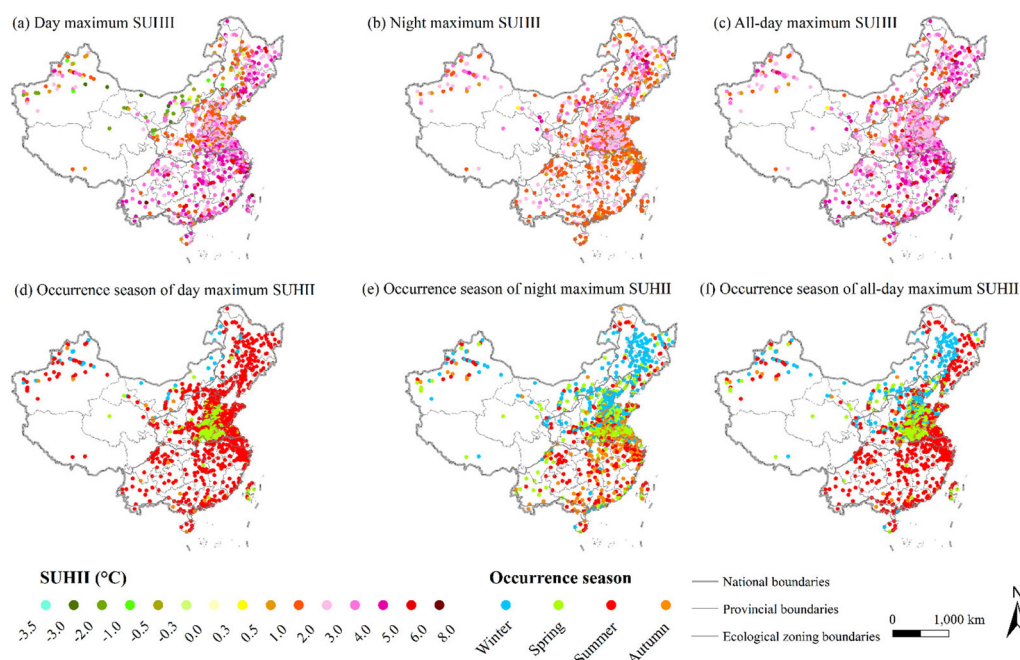


Figure 3. Distribution of the maximum surface urban heat island intensities (SUHII) (a–c) and the occurrence seasons (d–f) during the daytime, nighttime and all-day in China and its five ecological regions during 2015–2019.

The minimum SUHIIs were mostly negative in North China (region III < II < I). The values were mostly from -4.0 to -2.0 , -2.0 to -0.5 , -3.0 to -1.0 °C in the three regions mentioned above, respectively (Figures 4a, S5b, and S7a). Meanwhile, most of the minimum SUHIIs became positive in South China (region V = IV). The values were mostly from 0.5 to 2.0 and -0.5 to 2.0 °C in the two regions mentioned above, respectively. Moreover, the minimum SUHIIs occurred in the winter in 66.63% of cities in China (Figures 4d and S6b). From the region aspect, the minimum daytime SUHIIs mostly occurred in the winter in the hot and humid South China (regions V and IV), and region II, in the Spring and Autumn Seasons in regions I and III, and never in the summer in all regions except region III. In addition, the maximum and minimum of daytime SUHIIs were significantly correlated in all regions, especially in the hot and humid tropic region V ($r = 0.68$, $p < 0.05$) and subtropic region IV ($r = 0.50$, $p < 0.05$) (Figure 5).

The ranges of daytime SUHIIs were from 2 to 5 °C in 75.32% of cities in China. The order of regions in the daytime ranges of SUHIIs was region I > II = III > IV > V, in which the values mainly were from 4 to 6 , 3 to 5 , 2 to 5 , 2 to 4 , and 2 to 4 °C, respectively (Figures 6a, S8a, and S9). The maximum ranges of SUHIIs (>10 °C) were located in the five cities in Northeast China, while the minimum ranges (<1 °C) in the nine cities in dry West China and six cities in the southeast coastal regions of China.

4.1.2. Spatio-temporal changes of surface urban heat islands during the nighttime

The spatio-temporal variations of SUHIs during the nighttime were less than the daytime (Figures 2, S2, and S3). The annual mean SUHIIs were from 1 to 2 °C and negative in 53.43 and 2.47% urban region agglomerations, respectively (Figures 2f and S2f). These 23 urban region agglomerations with negative annual mean SUHIIs were discretely distributed in North China and the Yangtze River Basin. The order of regions was region II > III = V > I = IV (Figure S3b). The annual mean SUHIIs were mostly from 1 to 2 °C

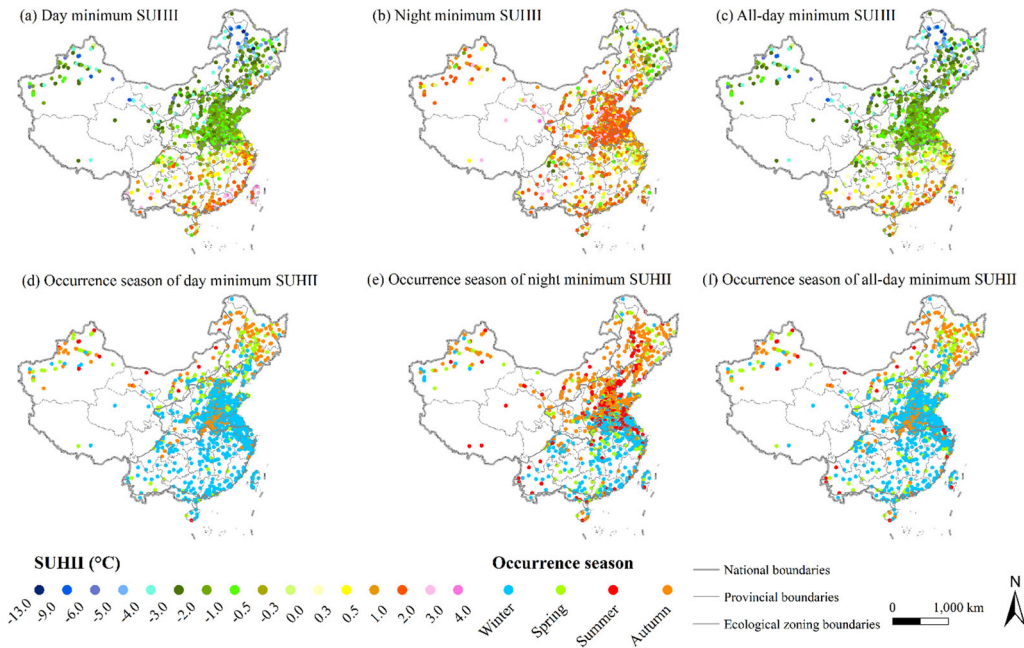


Figure 4. Distribution of the minimum surface urban heat island intensities (SUHII) (a–c) and the occurrence seasons (d–f) during the daytime, nighttime and all-day in China and its five ecological regions during 2015–2019.

	China	Region I	Region II	Region III	Region IV	Region V
Day maximum & minimum	0.57	0.43	0.38	0.38	0.5	0.68
Night maximum & minimum	0.56	0.3	0.69	0.61	0.54	0.67
All-day maximum & minimum	0.36	0.3	0.49	0.45	0.46	0.71
Day & night range	0.28	0.22	0.38	0.37	0.21	0.37

Figure 5. Spearman correlation coefficients between the maximum and minimum surface urban heat island intensities (SUHII) during the daytime, nighttime and all-day, and between the daytime and nighttime ranges of SUHII in China and its five ecological regions during 2015–2019. The symbol of “×” represented that the correlation coefficients have not passed the significant level of 0.05.

in all regions (Figure S2f). The largest seasonal variation occurred in region I (whose season order was winter > summer = spring > autumn) and least in region V (Figure S3b). Moreover, there were no significant differences in the mean nighttime SUHII during the spring and summer in all regions except in region IV.

The spatial variations were also lesser for the maximum and minimum SUHII during the nighttime than daytime (Figures 3 and S5). Their values were positive, and most from 1 to 3 °C in each region of China (Figures 3b and S4b). The maximum SUHII were significantly larger in North China than in South (Figure S5a). The variations were complex in the occurring seasons of the maximum nighttime SUHII (Figures 3e and S6a). These

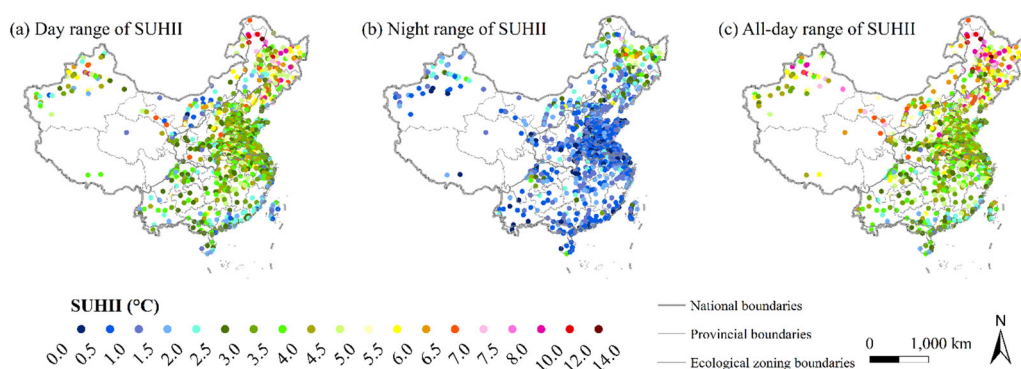


Figure 6. Distribution of the ranges of surface urban heat island intensities (SUHII) during the daytime, nighttime and all-day in China and its five ecological regions during 2015–2019.

maximum SUHII were most in the summer in region IV, in the autumn or spring in regions V and II, and in the winter in regions I and III.

The most minimum nighttime SUHII were from 0.0 to 2.0 °C in China (Figures 4b and S7b). The order of regions was region II > V = III > IV > I (Figure S5b). The largest values (>2.0 °C) were mostly located in some cities in the North Plain (Figure 4b). The minimum values were negative in 18.03% (168/932) urban region agglomerations, which could occur in each region, especially the humid regions I and IV. The minimum nighttime SUHII were most occurring in the winter in South China, while in the autumn in North China (Figures S6b and 5e). In addition, the maximum and minimum of nighttime SUHII were significantly correlated in all regions, especially in the hot and humid tropic region II ($r = 0.69$, $p < 0.05$) and subtropic region V ($r = 0.67$, $p < 0.05$) (Figure 5).

The spatial variations of SUHII ranges were less during the nighttime than daytime (Figures 6 and S8). The ranges of nighttime SUHII were from 0 to 2 °C in 83.15% of urban region agglomerations in China. The order of regions was region I > III > II = IV > V for the ranges of SUHII during the nighttime (Figure S9). The maximum ranges (>5 °C) were located in the 13 cities in Northeast China and three cities in regions II and III. Meanwhile, the minimum ranges (<0.5 °C) were mainly in some cities in the North Plain and southeast coastal areas.

4.1.3. Spatio-temporal changes of surface urban heat islands during the all-day period

The annual day-night differences (DNDs) of SUHII were generally larger and positive in South China (region IV > V), while smaller and negative in North China (region I > II > III) (Figures 2k, S2k and S3c). Obvious seasonal changes existed in these DNDs in each region. The day-night differences (DNDs) of SUHII were largest in the summer in all areas and when their mean values were positive in each region except region III in which the mean DNDs were always negative in the four seasons (Figure S3c). The largest DNDs were mainly located in the humid South and Northeast China in the summer. Meanwhile, these urban region agglomerations in each region had the lowest DNDs in the winter, and their regional mean values were all negative. It should note that no significance existed in the DNDs between during the winter and spring in region I, winter and spring or autumn in region III, autumn and spring in region V. Moreover, no significance existed between region IV and V for the DNDs in all seasons.

The largest maximum all-day SUHII were from 2 to 4 °C in 65.34% urban region agglomerations in China (Figures 3c and S4c). The values were larger in the hot and cold humid regions than in other regions (Figure S5). Meanwhile, the maximum all-day SUHII

values mostly occurred in the summer in the hot and cold humid regions, winter in the dry region III, and autumn in region II. Moreover, the spatial patterns of the minimum all-day SUHIs were quite similar to the daytime SUHIs (Figures 3 and S5). The larger differences between them were in some cities in humid and hot South China.

The minimum SUHIs during the all-day period were smaller than during the daytime, especially in the southeast coastal areas (Figures 4, S6 and S7). Moreover, 62.02% of urban region agglomerations owned the minimum SUHIs in the winter in the whole China (Figures 4f and S6b). From the region aspect, the minimum all-day SUHIs mostly occurred in the winter in the humid and hot South China (regions V and IV), and region II, in the Spring and Autumn Seasons in regions I and III, and never or least in the summer in all region except region V (Figure S6b). In addition, the relationships between the maximum and minimum values of the all-day SUHIs were insignificant ($p \geq 0.05$) in regions II and III, and significant in region I ($r = 0.30$), IV ($r = 0.46$) and V ($r = 0.71$) (Figure 5).

The spatial patterns and values of the SUHIs ranges during the all-day period were quite similar to them during the daytime. Moreover, the daytime ranges of SUHIs were insignificant with the nighttime values in most regions of China ($p > 0.05$) (Figure 6). In addition, the daytime SUHIs were insignificantly correlated with the nighttime values in 46.67% of cases for the urban region agglomerations in China and its four regions in the entire year and four seasons (Figure S10). However, the daytime SUHIs were significantly positively correlated with nighttime SUHIs in region V ($r \geq 0.44$ and $r \leq 0.58$) except in the winter.

4.2. Associated determinants of surface urban heat islands

The Δ EVI were significantly negatively partially correlated with SUHIs in the summer and the whole year in China, and insignificantly partially correlated with SUHIs in the winter in all regions. Moreover, the Δ EVI were significantly negatively and positively partially correlated with the SUHIs in the autumn and spring in regions II, IV and V, and the whole China, respectively ($p < 0.05$) (Figure 7a). It should note that regions IV and V were treated as a whole region (called region IV and V in this article) to study the associated determinants and simulation of SUHIs. The Δ EVI were significantly negatively partial correlated with SUHIs in the summer in each region ($p < 0.05$), in the whole year in all areas except region I, in the winter in regions II, IV and V, and the whole China, in the spring in region II and the whole China, and in the autumn in region IV and V. Significant positive relationships only existed in the autumn in region I (Figure 7b). The most obvious impacts occurred in the summer in region III ($r = -0.79$) and region I ($r = -0.61$). During the nighttime, the Δ EVI was significantly negatively partially correlated with SUHIs in the summer in each region ($p < 0.05$), in the whole year in all areas except region I, in the winter in region II, IV, and the whole China, in the spring in region II and the whole China, and in the autumn in region IV and V. Significant positive relationships only existed in the autumn in region I. The most obvious impacts occurred in the summer in region III ($r = -0.58$) and region IV and V ($r = -0.55$).

The Δ NLI was significantly positively and insignificantly partially with SUHIs, especially during the nighttime. The significant negative relationships existed in regions II and III during the winter daytime. The Δ Alb was most significantly with SUHIs during the nighttime in the summer, spring, and the whole year, and during the daytime in the spring and summer in China. These significant positive partial correlations usually occurred during the daytime in the summer, autumn and the entire year. The

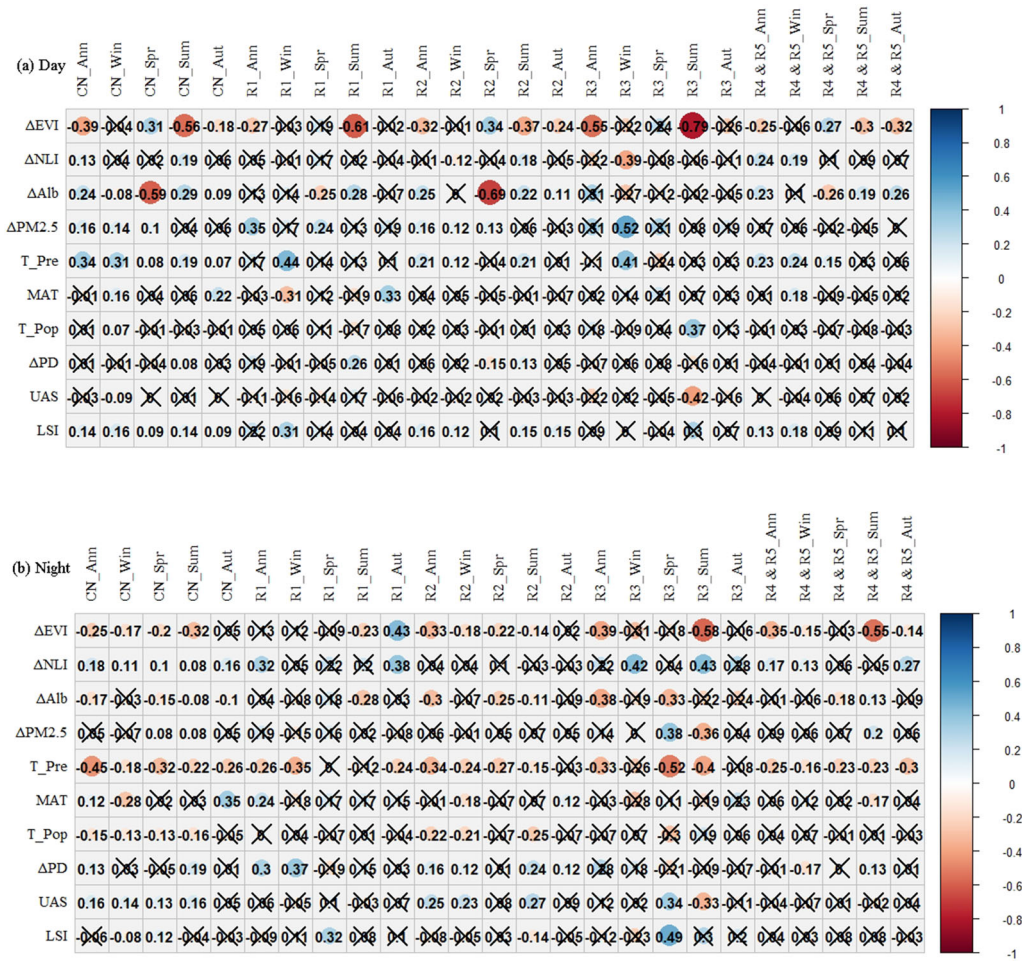


Figure 7. Partial correlation coefficients between mean surface urban heat island intensities and their drivers during the daytime and nighttime in China and its four ecological regions in the whole year and four seasons during 2015–2019. The symbol “×” represented that the partial correlation coefficients have not passed the significant level of 0.05. Regions IV and V were treated as a whole region (called region IV and V in this article) to analyze the associated determinants of SUHIs.

insignificant cases usually existed during the nighttime in the winter and autumn and during the daytime in region III. The impacts were most obvious in the spring in region II ($r = -0.69$). The $\Delta PM_{2.5}$ was insignificantly partially correlated with SUHIs in 16 of 25 and 20 of 25 cases during the daytime and nighttime, respectively. During the daytime, the significant positive relationships did not occur in the summer and in South China. The largest effect was in the winter in region III ($r = 0.52$). During the nighttime, four positive relationships occurred in the spring in region III ($r = 0.38$), in the summer in region IV and V ($r = 0.20$), and in the whole China in the spring and summer ($r = 0.08$). The T_Pre was significantly negatively and positively in 20 of 25 and 13 of 25 cases during the nighttime and daytime, respectively. The MAT was significantly positively and negatively partially with daytime SUHIs in 4 of 25 and 1 of 25 cases, respectively. Meanwhile, significant positive and negative relationships existed in 4 of 25 and 3 of 25 cases during the nighttime.

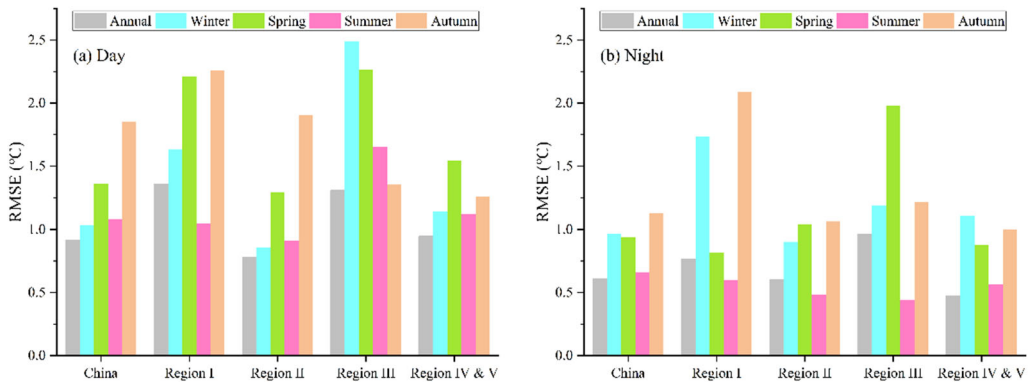


Figure 8. Simulation accuracies of surface urban heat island intensities in China and its four ecological regions in the whole year and four seasons based on the generalized regression neural network algorithm. RMSE meant the root-mean-square error. Regions IV and V were treated as a whole region (called region IV and V in this article) to simulate SUHIs.

The ΔPD was significantly positively partially correlated with the nighttime and daytime SUHIs in 9 of 25 and 3 of 25 cases, respectively, and negatively with them in 1 of 25 cases. The T_Pop was significantly positively and negatively partially with SUHIs in 2 of 25 and 7 of 25 cases, insignificantly in other cases. The UAS was insignificantly partially correlated with the daytime SUHIs in 23 of 25 cases and only significantly negatively with SUHIs in 2 of 25 cases. Meanwhile, the UAS was insignificantly partially correlated with the daytime SUHIs in 16 of 25 cases and only significantly positively and negatively in 8 of 25 and 1 of 25 cases, respectively. The LSI was significantly positively partially correlated with the daytime SUHIs in 12 of 25 cases. However, the impact was small in the vast majority of cases ($r < 0.18$) and largest in the winter in region I ($r = 0.31$). The significant positive and negative relationships only existed in 3 of 25 and 2 of 25 cases during the nighttime, respectively. The larger impacts occurred in the spring in region III ($r = 0.49$) and I ($r = 0.32$).

4.3. Simulation of surface urban heat islands

Both daytime and nighttime SUHIs could be well estimated in China and its four regions in the entire year and four seasons (Figure 8). The simulation accuracies were higher during the nighttime than daytime except in the winter in regions I and II. The RMSEs were less than 1.22°C in 88.00% of cases during the nighttime. The lowest and highest RMSEs were 0.44°C in region III in the summer and 2.09°C in region I in the autumn. Meanwhile, the RMSEs were less than 2.00°C in 76.00% of cases during the daytime. The lowest and highest RMSEs were 0.78°C in region II in the whole year and 2.40°C in region III in the winter.

5. Discussion

5.1. Quality control of the land surface temperatures using different methods

Some invalid LSTs exist in the MODIS product, which may be quite smaller than the true LSTs in these pixels and could probably cause some errors in calculating SUHIs. Therefore, it was necessary and important to remove them, especially when using the MODIS LSTs data under bad meteorological conditions. During the summer daytime,

such four images were chosen, including four images on the 153rd day in region IV, 193rd day in region II, 225th day in region V, and 241th day in region I and III in 2020. We could distinguish these invalid LSTs easily in these images because the true LSTs were usually positive and large during this period in the vast majority of regions in China except in some southwestern mountain regions with high altitudes. Moreover, only the daytime data were analyzed in this study because the accuracies of LSTs were usually lower during the daytime than nighttime. Seven methods were adopted to control the LSTs quality, including two methods used in previous research (Clinton and Gong 2013; Wang et al. 2018) and five proposed by ourselves (Table S3). The stratified sampling method was adopted to create 30,000 samples to estimate the performances of these methods, including 1000 points in each region and land use. There were five regions and six land uses here, including cropland, woodland, grassland, waterbody, built-up land and unused land (Zhang et al. 2014).

The percentages of invalid LSTs derived by the visual interpretation were 15.93, 6.83, 4.05, 6.18 and 24.83% in the five regions. Those invalid LSTs were mainly affected by bad weather conditions. They were seldomly related to the land use types. But a few of them could distribute in the ecotone of land and waterbodies. The first method could not basically identify the invalid LSTs at all (Figure S11). The second method could find about 12.71% invalid values in most regions of China except region II, but eliminated the right LSTs with the proportion from 24.20% in region III to 90.58% in region V. The percentages of invalid grids that were correctly identified continued to increase from 46.77% using the third method to 100.00% by the seventh method. Meanwhile, the percentage of valid grids that were wrongly removed increased from 9.42 to 18.96%. We encouraged the quality of LSTs should be controlled at least using the fourth method for the SUHIs research in the future. Moreover, our results showed that some invalid LSTs could not be removed only using the search method within horizontal or eight directions, especially for the clusters of invalid values with large areas.

5.2. Significance of findings of the spatio-temporal changes rules of surface urban heat islands

The daytime SUHIs were largest in the hot summer in all regions, which was consistent with previous research (Yao et al. 2017; Peng et al. 2018; Ma et al. 2021). During the summer daytime, the hot and cold humid regions had higher SUHIs than other regions. This was similar to previous work, in which during the summer days, the SUHI in Northeast China and Southwest China was the highest, with the median of 2.64 and 2.14 °C, respectively (Ma et al. 2021). Meanwhile, the daytime SUHIs were least in the winter in regions II, IV and V, and in the Spring and Autumn seasons in regions I and III. Moreover, the minimum nighttime SUHIs were most in the winter in South China. These findings indicated that the SUHIs in China could decrease temperature-related comfort, increase the energy consumption required for cooling and heating, and lead to more emissions of warm gases and atmospheric pollutants.

Both urban heat islands and sinks were possible in the same location for many global cities, though timing may differ by the qualitative observation method (Clinton and Gong 2013). Nevertheless, the maximum and minimum SUHIs were significantly positively correlated in all regions during the daytime and nighttime ($p < 0.05$) in our work. The results indicated that it was difficult for humans to decrease the maximum SUHIs while increasing the minimum SUHIs simultaneously. This finding was more crucial during the daytime. The maximum daytime SUHIs were most occurring in the hot summer in

all regions of China. Meanwhile, the minimum SUHIs mostly occurred in the winter in the hot and humid South China (regions V and IV), and region II, and in the Spring and Autumn Seasons in regions I and III. Besides, the daytime ranges of SUHIs were insignificant with the nighttime values in most regions of China ($p \geq 0.05$). Moreover, the daytime SUHIs were insignificantly correlated with the nighttime values in 46.67% of cases for the urban region agglomerations in China and its four regions in the entire year and four seasons. This was consistent with previous research, which found no significant correlation existed between daytime and nighttime annual SUHI across 419 global big cities (Peng et al. 2012). These results showed that the mechanisms were different for the SUHIs during the daytime and nighttime. They should be studied and considered separately in future work. The related descriptions were added as follows. Air temperatures have more direct impacts on human thermal comfort than LSTs. Although the LSTs were closely associated with temperature (Schwarz et al. 2011; Ho et al. 2016; Bechtel et al. 2017), it was still impossible to obtain satisfactory results by directly converting them under the urban context. Therefore, the SUHIs cannot be directly comparable to air UHIs (Voogt and Oke 2003; Zhou et al. 2019). In the future, the urban temperature prediction should be strengthened based on the land surface temperature, landscape composition and pattern, surface biophysical parameters, etc. (Hengl et al. 2012; Ho et al. 2016).

5.3. Associated determinants of surface urban heat islands

5.3.1. Vegetation activity

During the daytime (the morning), ΔEVI generally could mitigate SUHIs due to the vegetation transpiration, especially under the conditions with more and denser vegetation, such as in the summer in all regions and in the autumn in region II and South China. This finding was consistent with the previous study (Yao et al. 2017). No significant relationships existed in each region in the winter, mainly due to the least vegetation activities. It should note ΔEVI was significantly positively partially correlated with the daytime SUHIs in the spring in regions II, IV and V. One previous study has found the positive correlations existed in certain cities in North China during the winter daytime (Yao et al. 2017). They inferred the reason might be the spurious EVI values. The detailed mechanism needed to be studied further.

During the nighttime, the grasses (especially short grasses) generally had lower LSTs than the urban land because of the large sky view factor (SVF), low heat capacity, the mixture of bare soil, gravel, and other inert materials (Kim 1992; Chudnovsky et al. 2004; Chen 2017). However, the impacts of forests on LSTs were complex during the nighttime. On the one hand, the forests could decrease the LSTs because the shading effects of trees could reduce the amount of heat stored during the daytime and reduce the nighttime LSTs (Tiangco et al. 2008; Quan et al. 2016; Yao et al. 2017). Moreover, the LSTs could be lowered due to the considerable amount of evapotranspiration during the nighttime, especially in tropical forests (Li et al. 2015). On the other hand, the forests may increase the LSTs due to the small SVF (Chudnovsky et al. 2004; Li et al. 2019b), the stored energy within and beneath canopies during the daytime, and the re-emitted longwave radiation from both the vegetation canopy and the underlying ground during the nighttime (Chudnovsky et al. 2004; Li et al. 2019b), etc. In this study, the ΔEVI was significantly negatively partially correlated with SUHIs in most cases, especially under conditions with more and denser vegetations. One reason may be the most cities were surrounded by farmland, and the thermal characters of crops were quite similar to the grasslands. The insignificant cases mainly occurred in the dry region III and cold region I in the winter

and Spring Autumn Seasons. Only one positive relationship existed in region I in the autumn.

5.3.2. Anthropogenic heat emissions

The Δ NLI was usually used to indicate the anthropogenic heat flux, enhancing the SUHII during the daytime (Peng et al. 2012; Chen et al. 2016; Yao et al. 2017) and nighttime (Peng et al. 2012; Zhou et al. 2014; Yao et al. 2017). Meanwhile, the previous research found that the Δ NLI was not significantly partially correlated with daytime SUHII in the global 419 large cities in the winter and summer (Peng et al. 2012) and 32 major cities of China in the winter (Zhou et al. 2014). The Δ NLI was insignificantly correlated with the daytime and nighttime SUHII in the winter and summer and negative with the daytime SUHII in the winter and summer in 31 major cities of China (Yao et al. 2017). Our study was consistent with the previous research. The significant positive and insignificant correlations commonly existed. Two negative cases existed during the winter daytime in regions II and III.

5.3.3. Albedo

Materials with smaller albedos could absorb more energy during the daytime and emit them during the nighttime, resulting in higher air and surface temperatures during the nighttime in most research (Jin et al. 2005; Peng et al. 2012; Zhou et al. 2014; Cao et al. 2016). Nevertheless, the relationships were complex during the daytime. All insignificant and significant positive and negative relationships existed in previous research (Peng et al. 2012; Zhou et al. 2014; Quan et al. 2016; Duncan et al. 2019). Our results were consistent with these findings.

5.3.4. Aerosol pollution

Aerosols could affect the urban heat island intensities (UHII) by changing the surface energy balance by the aerosol radiative effect (ARE) and planetary-boundary-layer (PBL) stability and airflow intensity by modifying the thermodynamic structure, which was referred to as the aerosol dynamic effect (ADE) (Cao et al. 2016; Han et al. 2020). The ARE included not only the absorption and emitting of radiation in the longwave atmospheric spectrum but also the reduction of the shortwave radiation that reached the ground surface (Jacobson 1998; Cao et al. 2016). The annual nighttime SUHII could be obviously enhanced by haze pollution in China (Cao et al. 2016). The aerosols could increase and reduce the UHII during the winter and summer daytime in China dominated by the ARE and ADE, respectively (Han et al. 2020). The Δ PM_{2.5} could slightly enhance the annual daytime SUHII in China (Niu et al. 2021b). The effects of air pollutions were larger in the cities in semi-arid climates than in humid climates because the coarser aerosols could result in higher longwave radiative forcing (Cao et al. 2016; Li et al. 2019b). Our results were consistent with these findings to some degree. For instance, the Δ PM_{2.5} could enhance SUHII significantly in some cases during the daytime and nighttime. The largest effects were located in the dry region III during the daytime and nighttime. However, some differences also existed. The insignificant rather than the significant negative relationships were found in the summer daytime in this study.

5.3.5. Climate

The precipitation could enlarge the soil moisture (especially in the rural regions) and further increase the differences of thermal inertia between the urban and rural regions. Therefore, T_{Pre} could mitigate and enhance the SUHII during the nighttime and

daytime, respectively (Peng et al. 2012; Cao et al. 2016; Zhou et al. 2016; Yao et al. 2018; Li et al. 2019b). Our study verified this.

The effects of MAT were complex on the daytime and nighttime SUHIs. Our findings were consistent with previous research, in which all the insignificant, significant positive and negative relationships existed (Peng et al. 2012; Zhou et al. 2014; Cao et al. 2016; Zhou et al. 2016; Yao et al. 2018).

5.3.6. Population

Population density is a more effective indicator of the impact of human activities on local climate per unit area than the total population. Therefore, the ΔPD has more direct impacts on SUHIs than T_Pop and was a more appropriate indicator than T_Pop, but was rarely used (Peng et al. 2012; Li et al. 2019b). We have found the ΔPD had significant positive impacts on SUHIs in some cases, especially during the nighttime, and negative in one case during the daytime or nighttime. The results were consistent with previous research, but some differences still existed. The ΔPD was insignificantly correlated with the daytime and nighttime SUHIs in the winter, summer, and the entire year for 419 big global cities (Peng et al. 2012). Moreover, the significant positive partial correlations existed in some cases during the nighttime, especially in South China ($p < 0.01$) in a previous study whose study objects included the 1449 urban region clusters in China (Li et al. 2019b). Only two significant negative relationships existed during the daytime (Li et al. 2019b). These differences were mainly caused by the different study objects, observation times, population data, etc.

The T_Pop was usually used to indicate the population effects on SUHIs using the correlation analysis method in many previous researches. However, two limitations existed. On the one hand, the T_Pop has neglected the population density between the urban and rural regions. On the other hand, the correlation method only considers two variables and omits other influencing factors' roles, and thus leading to a certain bias or errors. For instance, significant correlations were found between SUHIs and T_Pop in the vast majority of cases during the daytime and nighttime in the 1449 urban region clusters (Li et al. 2019b). Nevertheless, no significant partial correlations existed during the daytime, and the significant positive ones only occurred in 4 of 25 cases during the nighttime (Li et al. 2019b). Our study was consistent with the previous findings, in which the T_Pop showed poor explanation ability to the daytime and nighttime SUHIs.

5.3.7. Urban area size and shape

The UAS was usually significantly positively correlated with SUHIs (Li et al. 2019b) and foot-print areas (Zhou et al. 2015). But the partial correlations were quite weak between UAS and SUHIs (Peng et al. 2012; Zhou et al. 2014; Li et al. 2019b). Our findings were consistent with these previous conclusions to some degree. The UAS was insignificant partially correlated with daytime and nighttime SUHIs in 23 of 25 and 16 of 25 cases, respectively. Nevertheless, the UAS had significant positive effects on nighttime SUHIs in 8 of 25 cases. The LSI could significantly enhance the daytime SUHIs in some cases in China except in region III. The mechanism needed to be studied further. Although the impacts of urban shape were usually minor, the urban planners should consider designing the urban regions with more simple shapes to mitigate SUHIs.

5.4. Simulation of SUHIs

It is crucial to realize the simulation of SUHIs with high accuracy by simple methods using a small number of highly accessible indicators. To our knowledge, this research was very scarce, which focused on the SUHIs of many cities at a large scale simply by using several key influencing factors and did not adopt the complex and professional climatology model (Wang et al. 2015; Li et al. 2019b). No significant differences existed between these simulated SUHIs using three different indicators (including all potential drivers or only these drivers that were significantly correlated or partially correlated with the SUHIs) and four machine learning methods (including the GRNN and three Support Vector Machine algorithms based on the genetic algorithm, particle swarm optimization, and grid search methods) (Li et al. 2019b). Therefore, this study simulated SUHIs only using these drivers, which were partially correlated with SUHIs in most cases. We used all drivers to estimate these SUHIs when no influences were significant with SUHIs. Moreover, all influencing factors adopted in this study could be easily accessed. In addition, their values could be specific to each grid. Both daytime and nighttime SUHIs could be well estimated in all papers and the simulation accuracies were generally higher during the night than daytime. The high simulation accuracies in the research could indicate the urban planners could consider the SUHI issue by managing several key determinants, which is quite helpful for monitoring, assessing, and optimizing the urban thermal environment.

6 Conclusions

We studied the spatio-temporal variations and ten associate determinants of SUHIs during the morning (~10:30 am) and before midnight (~10:30 pm) of 932 urban region agglomerations in the five regions with different ecological contexts in China and further simulated these SUHIs. Some important conclusions can be summarized as follows:

1. It was necessary and important to remove these invalid LSTs to study SUHIs. The proposed QC method of LSTs could identify almost all wrong values effectively while eliminating the valid LSTs as little as possible.
2. The daytime SUHIs were largest in the hot summer in all regions when the hot and cold humid regions had higher SUHIs than other regions. Meanwhile, the SUHIs were least in the winter in regions II, IV and V and in the Spring and Autumn Seasons in regions I and III. The minimum nighttime SUHIs were most in the winter in South China. Besides, the maximum and minimum SUHIs were significantly positively correlated in all regions during the daytime and nighttime. Moreover, the daytime ranges of SUHIs were insignificant with the nighttime values in most regions of China ($p > 0.05$). The daytime SUHIs were insignificantly correlated with the nighttime values in 46.67% of cases.
3. The ΔEVI was generally significantly negatively partially correlated with the daytime and nighttime SUHIs, while the ΔNLI was positively partially correlated with them in some cases. The ΔAlb was significantly negatively partially with some nighttime SUHIs. The $\Delta\text{PM}_{2.5}$ was significantly positively partially correlated with 9 of 25 daytime and 4 of 25 nighttime SUHIs, respectively. The largest effects of $\Delta\text{PM}_{2.5}$ on SUHIs were occurring in the dry region III during both the daytime and nighttime. The T_{Pre} was significantly negatively and positively partially correlated with SUHIs in most cases during the nighttime and daytime, respectively. The ΔPD was

significantly positively partially correlated with nighttime and daytime SUHIs in 9 of 25 and 3 of 25 cases, respectively. The UAS and LSI were significantly positively partially correlated with the nighttime SUHIs in 8 of 25 cases and daytime SUHIs in 12 of 25 cases.

4. Both daytime and nighttime SUHIs could be well estimated in China and its four regions in the entire year and four seasons. The simulation accuracies were higher during the nighttime than daytime except in the winter in regions I and II. The RMSEs were less than 1.22 °C in 88.00% and less than 2.00 °C in 76.00% of cases during the nighttime and daytime, respectively.
5. One contribution of the present research was to improve the research framework and methods of SUHIs, including proposing a method to remove the invalid values of LSTs data, developing a two-step aggregation method to extract the urban regions accurately, analysing the spatial-temporal changes of SUHIs by several aspects during the morning and before midnight, exploring ten associated determinants for these SUHIs, including the PM_{2.5}, urban shape, etc., and simulating SUHIs accurately by the GRNN algorithm. Another significance was to obtain the corresponding results by the methods mentioned above, which can help master the status of SUHIs accurately, assess the positive and negative effects of urban heat islands comprehensively, regulate and optimize SUHIs scientifically and predictably, etc.

Disclosure statement

The authors have no relevant financial or non-financial interests to disclose.

Funding

This research was funded by the Natural Science Foundation of China (Grant No. 41901235), Key Scientific Research Project of Universities and Colleges of Henan Province (Grant No. 21A170005), Henan Provincial Youth Natural Science Foundation (Grant No. 212300410103), Key Scientific and Technological Research Projects of Henan Province (Grant No. 212102310005 & No.192102310274), Key Scientific and Technological Project of Education Department of Henan Province (Grant No. 202102310337).

Data availability

The data in this study are available from the corresponding author upon request.

References

- Bechtel B, Zakšek K, Oßenbrügge J, Kaveckis G, Böhner J. 2017. Towards a satellite based monitoring of urban air temperatures. *Sustain Cities Soc.* 34:22–31.
- Cao C, Lee X, Liu S, Schultz N, Xiao W, Zhang M, Zhao L. 2016. Urban heat islands in China enhanced by haze pollution. *Nat Commun.* 7:12509.
- Chakraborty T, Lee X. 2019. A simplified urban-extent algorithm to characterize surface urban heat islands on a global scale and examine vegetation control on their spatiotemporal variability. *Int J Appl Earth Obs Geoinf.* 74:269–280.
- Chen K, Newman AJ, Huang M, Coon C, Darrow LA, Strickland MJ, Holmes HA. 2022. Estimating heat-related exposures and urban heat island impacts: A case study for the 2012 Chicago heatwave. *Geohealth*6(1):e2021GH000535.
- Chen L, Jiang R, Xiang W. 2016. Surface heat island in Shanghai and its relationship with urban development from 1989 to 2013. *Adv Meteorol.* 2016:1–15.

- Chen T. 2017. Studies on spatiotemporal dynamics of thermal radiation temperatures of different landscapes in Beijing city. Hefei: University of Science and Technology of China.
- Chudnovsky A, Ben-Dor E, Saaroni H. 2004. Diurnal thermal behavior of selected urban objects using remote sensing measurements. *Energy Build.* 36(11):1063–1074.
- Clinton N, Gong P. 2013. MODIS detected surface urban heat islands and sinks: Global locations and controls. *Remote Sens Environ.* 134:294–304.
- Duncan J, Boruff B, Saunders A, Sun Q, Hurley J, Amati M. 2019. Turning down the heat: An enhanced understanding of the relationship between urban vegetation and surface temperature at the city scale. *Sci Total Environ.* 656:118–128.
- Han W, Li Z, Wu F, Zhang Y, Guo J, Su T, Cribb M, Fan J, Chen T, Wei J, et al. 2020. The mechanisms and seasonal differences of the impact of aerosols on daytime surface urban heat island effect. *Atmos Chem Phys.* 20(11):6479–6493.
- Hengl T, Heuvelink G, Tadi MP, Pebesma EJ. 2012. Spatio-temporal prediction of daily temperatures using time-series of MODIS LST images. *Theor Appl Climatol.* 107(1–2):265–277.
- Ho HC, Knudby A, Xu Y, Hodul M, Aminipouri M. 2016. A comparison of urban heat islands mapped using skin temperature, air temperature, and apparent temperature (Humidex), for the greater Vancouver area. *Sci Total Environ.* 544(15):929–938.
- Imhoff ML, Zhang P, Wolfe RE, Bounoua L. 2010. Remote sensing of the urban heat island effect across biomes in the continental USA. *Remote Sens Environ.* 114(3):504–513.
- Jacobson MZ. 1998. Studying the effects of aerosols on vertical photolysis rate coefficient and temperature profiles over an urban airshed. *J Geophys Res.* 103(D9):10593–10604.
- Jan M, Dickinson RE, Zhang D. 2005. The footprint of urban areas on global climate as characterized by MODIS. *J Clim.* 18(10):1551–1565.
- Kim HH. 1992. Urban heat island. *Int J Remote Sens.* 13(12):2319–2336.
- Lai J, Zhan W, Huang F, Voogt J, Bechtel B, Allen M, Peng S, Hong F, Liu Y, Du P. 2018. Identification of typical diurnal patterns for clear-sky climatology of surface urban heat islands. *Remote Sens Environ.* 217:203–220.
- Lai J, Zhan W, Quan J, Bechtel B, Wang K, Zhou J, Huang F, Chakraborty T, Liu Z, Lee X. 2021. Statistical estimation of next-day nighttime surface urban heat islands. *ISPRS J Photogramm Remote Sens.* 176:182–195.
- Li Y, Li J, Xu A, Feng Z, Hu CH, Zhao G. 2021. Spatial-temporal changes and associated determinants of global heating degree days. *Int J Environ Res Public Health.* 18(12):6186.
- Li Y, Wang L, Liu M, Zhao G, He T, Mao Q. 2019b. Associated determinants of surface urban heat islands across 1449 cities in China. *Adv Meteorol.* 2019:1–14.
- Li Y, Wang L, Zhang L, Liu M, Zhao G. 2019a. Monitoring intra-annual spatiotemporal changes in urban heat islands in 1449 cities in China based on remote sensing. *Chin Geogr Sci.* 29(6):905–916.
- Li Y, Zhao M, Motesharrei S, Mu Q, Kalnay E, Li S. 2015. Local cooling and warming effects of forests based on satellite observations. *Nat Commun.* 6:6603.
- Liu H, Huang B, Zhan Q, Gao S, Li R, Fan Z. 2021. The influence of urban form on surface urban heat island and its planning implications: Evidence from 1288 urban clusters in China. *Sustain Cities Soc.* 71:102987.
- Liu J, Kuang W, Zhang Z, Xu X, Qin Y, Ning J, Zhou W, Zhang S, Li R, Yan C, et al. 2014. Spatiotemporal characteristics, patterns, and causes of land-use changes in China since the late 1980s. *J Geogr Sci.* 24(2):195–210.
- Lloyd CT, Sorichetta A, Tatem AJ. 2017. High resolution global gridded data for use in population studies. *Sci Data.* 4(1):170001
- Niu L, Peng Z, Tang R, Zhang Z. 2021a. Development of a long-term dataset of China surface urban heat island for policy making: Spatio-temporal characteristics. In *Proceedings of the 2021 IEEE International Geoscience and Remote Sensing Symposium IGARSS, Brussels, Belgium, July 11–16*; p. 6928–6931.
- Niu L, Zhang Z, Peng Z, Liang Y, Liu M, Jiang Y, Wei J, Tang R. 2021b. Identifying surface urban heat island drivers and their spatial heterogeneity in China's 281 cities: an empirical study based on multi-scale geographically weighted regression. *Remote Sens.* 13(21):4428.
- Ma L, Wang Y, Liang Z, Ding J, Shen J, Wei F, Li S. 2021. Changing effect of urban form on the seasonal and diurnal variations of surface urban heat island intensities (suhii) in more than 3000 cities in China. *Sustainability.* 13(5):2877.
- Marzban F, Soudoudi S, Preusker R. 2018. The influence of land-cover type on the relationship between NDVI–LST and LST–Tair. *Int J Remote Sens.* 39(5):1377–1398.

- Mohanty MP, Simonovic SP. 2021. Understanding dynamics of population flood exposure in Canada with multiple high-resolution population datasets. *Sci Total Environ.* 759:143559.
- Peng J, Ma J, Liu Q, Liu Y, Hu Y, Li Y, Yue Y. 2018. Spatial-temporal change of land surface temperature across 285 cities in China: an urban-rural contrast perspective. *Sci Total Environ.* 635(1):487–497.
- Peng S, Piao S, Ciais P, Friedlingstein P, Ottle C, Bréon FO-M, Nan H, Zhou L, Myneni RB. 2012. Surface urban heat island across 419 global big cities. *Environ Sci Technol.* 46(2):696–703.
- Peng S, Piao S, Ciais P, Friedlingstein P, Ottle C, Bréon F-M, Nan H, Zhou L, Myneni RB. 2012. Response to comment on “Surface Urban Heat Island Across 419 Global Big Cities”. *Environ Sci Technol.* 46(12):6889–6890.
- Quan J, Zhan W, Chen Y, Wang M, Wang J. 2016. Time series decomposition of remotely sensed land surface temperature and investigation of trends and seasonal variations in surface urban heat islands. *J Geophys Res Atmos.* 121(6):2638–2657.
- Rigo G, Parlow E, Oesch D. 2006. Validation of satellite observed thermal emission with in-situ measurements over an urban surface. *Remote Sens Environ.* 104(2):201–210.
- Rooki R. 2016. Application of general regression neural network (GRNN) for indirect measuring pressure loss of Herschel–Bulkley drilling fluids in oil drilling. *Measurement.* 85:184–191.
- Schwarz N, Lautenbach S, Seppelt R. 2011. Exploring indicators for quantifying surface urban heat islands of European cities with MODIS land surface temperatures. *Remote Sens Environ.* 115(12):3175–3186.
- Sfîcă L, Ichim P, Apostol L, Ursu A. 2018. The extent and intensity of the urban heat island in Iai city. *Theor Appl Climatol.* 134(3–4):777–791.
- Shen Z, Shi J, Tan J, Yang H. 2020. The migration of the warming center and urban heat island effect in Shanghai during urbanization. *Front Earth Sci.* 8:340.
- Silva V, Silva C, Almeida L, Silva C, Carvalho H, Camargo R. 2018. Mobile transect for identification of intra-urban heat islands in Uberlandia, Brazil. *Rev Ambiente Água.* 13(4):e2187–e2187.
- Tiangco M, Lagmay A, Argete J. 2008. ASTER-based study of the night-time urban heat island effect in Metro Manila. *Int J Remote Sens.* 29(10):2799–2818.
- United Nations, Department of Economic and Social Affairs (UN DESA). 2014. World Urbanization Prospects: The 2014 Revision, Highlights. Department of Economic and Social Affairs. Population Division, United Nations.
- Voogt JA, Oke TR. 2003. Thermal remote sensing of urban climates. *Remote Sens Environ.* 86(3):370–384.
- Wan Z. 2008. New refinements and validation of the MODIS Land-Surface Temperature/Emissivity products. *Remote Sens Environ.* 112(1):59–74.
- Wang J, Huang B, Fu D, Atkinson P. 2015. Spatiotemporal variation in surface urban heat island intensity and associated determinants across major Chinese cities. *Remote Sens.* 7(4):3670–3689.
- Wang J, Meng B, Fu D, Pei T, Xu C. 2018. Mapping spatiotemporal patterns and multi-perspective analysis of the surface urban heat islands across 32 major cities in China. *ISPRS Int J Geo-Inf.* 7(6):207.
- Wei J, Li Z, Cribb M, Huang W, Xue W, Sun L, Guo J, Peng Y, Li J, Lyapustin A, et al. 2020. Improved 1 km resolution PM_{2.5} estimates across China using enhanced space-time extremely randomized trees. *Atmos Chem Phys.* 20(6):3273–3289.
- Wei J, Li Z, Lyapustin A, Sun L, Peng Y, Xue W, Su T, Cribb M. 2021. Reconstructing 1-km-resolution high-quality PM_{2.5} data records from 2000 to 2018 in China: spatiotemporal variations and policy implications. *Remote Sens Environ.* 252:112136.
- Yang Q, Huang X, Li J. 2017. Assessing the relationship between surface urban heat islands and landscape patterns across climatic zones in China. *Sci Rep.* 7(1):9337.
- Yang Q, Huang X, Tang Q. 2019. The footprint of urban heat island effect in 302 Chinese cities: temporal trends and associated factors. *Sci Total Environ.* 655:652–662.
- Yao R, Wang L, Huang X, Liu Y, Niu Z, Wang S, Wang L. 2021. Long-term trends of surface and canopy layer urban heat island intensity in 272 cities in the mainland of China. *Sci Total Environ.* 772(3):145607.
- Yao R, Wang L, Huang X, Niu Z, Liu F, Wang Q. 2017. Temporal trends of surface urban heat islands and associated determinants in major Chinese cities. *Sci Total Environ.* 609:742–754.
- Yao R, Wang L, Huang X, Zhang W, Li J, Niu Z. 2018. Interannual variations in surface urban heat island intensity and associated drivers in China. *J Environ Manage.* 222(15):86–94.
- Zhang P, Imhoff M, Wolfe R, Bounoua L. 2010. Characterizing urban heat islands of global settlements using MODIS and nighttime lights products. *Can J Remote Sens.* 36(3):185–196.
- Zhang Z, Wang X, Zhao X, Liu B, Yi L, Zuo L, Wen Q, Liu F, Xu J, Hu S. 2014. A 2010 update of National Land Use/Cover Database of China at 1:100000 scale using medium spatial resolution satellite images. *Remote Sens Environ.* 149:142–154.

- Zhou D, Xiao J, Bonafoni S, Berger C, Deilami K, Zhou Y, Froking S, Yao R, Qiao Z, Sobrino J. 2019. Satellite remote sensing of surface urban heat islands: progress, challenges, and perspectives. *Remote Sens.* 11(1):11010048.
- Zhou D, Zhang L, Li D, Huang D, Zhu C. 2016. Climate–vegetation control on the diurnal and seasonal variations of surface urban heat islands in China. *Environ Res Lett.* 11(7):074009.
- Zhou D, Zhao S, Liu S, Zhang L, Chao Z. 2014. Surface urban heat island in China's 32 major cities: spatial patterns and drivers. *Remote Sens Environ.* 152:51–61.
- Zhou D, Zhao S, Zhang L, Sun G, Liu Y. 2015. The footprint of urban heat island effect in China. *Sci Rep.* 5:11160.